Engineering Fracture Mechanics 270 (2022) 108568

Contents lists available at ScienceDirect

Engineering Fracture Mechanics

journal homepage: www.elsevier.com/locate/engfracmech

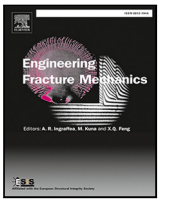

Fracture-based transient thermo-mechanical analysis of reciprocating engine thermal barrier coatings

G. Koutsakis [a,*], M.R. Begley [b], J.W. Hutchinson [c], J.B. Ghandhi [a]

[a] Engine Research Center, University of Wisconsin–Madison, WI, USA
[b] Materials Department, University of California Santa Barbara, Santa Barbara, CA, USA
[c] School of Engineering and Applied Sciences, Harvard University, Cambridge MA, USA

ARTICLE INFO

Keywords:
Internal combustion engine
Thermal barrier coating
Fracture mechanics
Delamination
Energy release rate

ABSTRACT

The durability of thermal barrier coatings for reciprocating internal combustion engine applications was investigated using a coupled, unsteady fracture-based thermomechanics model. The intra-cycle engine heat flux varies substantially in magnitude and has frequency similar to that of the coating thermal timescale, giving rise to relatively large spatial temperature nonuniformity within the coating that varies temporally. A finite difference scheme was used to calculate the temperature field. An analytical model that assumes equi-biaxial stress followed by plane strain delamination was used to evaluate an energy release rate that represents the driving force for cracking. Because the location and time of the peak energy release rate cannot be established *a priori*, they were computed for all times in the cycle. The peak energy release rate was found to occur later in the cycle than the peak surface temperature, and was often located within the coating as compared to at the coating–substrate interface where there was a mismatch in coefficient of thermal expansion. Coating thickness was found to affect both the magnitude of the peak energy release rate and its location. The residual stress, which arises from the coating deposition process, was found to have a significant effect on the peak energy release rate, and may be a process parameter that can be used to promote coating life. The computational framework demonstrated insight regarding the trade-off between engine thermodynamic performance and coating durability.

1. Introduction

Propulsion systems and spacecraft reentry vehicles often use protective coatings for components exposed to extreme thermal conditions because most structural materials do not exhibit sufficient thermal performance, and vice versa. Multilayer architectures allow an appropriate balance, specific to the application, between thermal properties, stored strain energy arising from thermal misfit, and adhesion. Arguably, thermal barrier coatings in gas turbines represent the most advanced coating systems, and have enabled dramatic gains in efficiency by allowing higher turbine inlet temperatures.

The heat transfer characteristics in reciprocating internal combustion engines are significantly different than gas turbine propulsion systems, suggesting that advanced gas turbine coatings cannot be directly used in combustion engines. Unlike gas turbines, reciprocating engine heat transfer is highly unsteady. Three distinct frequency ranges can be identified. The lowest frequency range ($\sim 10^{-3} - 10^{-2}$ Hz) occurs during the engine start-up or shutdown, where a slow heating or cooling process occurs. The intermediate range ($\sim 10^{-1}$ Hz) corresponds to sudden load/speed changes during operation. The highest frequency range

* Corresponding author.
E-mail address: koutsakis@wisc.edu (G. Koutsakis).

https://doi.org/10.1016/j.engfracmech.2022.108568
Received 7 March 2022; Received in revised form 4 May 2022; Accepted 20 May 2022
Available online 2 June 2022
0013-7944/Published by Elsevier Ltd.

Nomenclature

$\dot{q}''$	Heat Flux [Wm^{-2}]
t	Temperature [K]
k	Thermal Conductivity [$Wm^{-1}K^{-1}$]
ρ	Density [kgm^{-3}]
c	Specific heat capacity [$Jkg^{-1}K^{-1}$]
L	Length [m]
σ	Stress [Pa]
α	Coefficient of Thermal Expansion [K^{-1}]
ν	Poisson Ratio [-]
E	Young's Modulus [GPa]
$\bar{E}$	Effective moduli [GPa]
θ	Thermal strain [-]
$\bar{c}$	θ coefficient [-]
ϵ	Total strain [-]
κ	Curvature [m^{-1}]
a_{ij}, b_{ij}	Deformation analysis coefficients [-]
ℓ_i	Element Thickness [m]
H_b	Bottom sub-multilayer height [m]
x	Position x [m]
y	Position y [m]
N	Number of nodes [-]
U	Strain energy [Jm^{-2}]
G	Energy Release Rate [Jm^{-2}]
G_c	Toughness [Jm^{-2}]

Subscripts

i	index
t	top
b	bottom
x	x-direction
y	y-direction
z	z-direction

Subscripts

ref	reference
w	whole
t	top
b	bottom

($\sim$ 1 – 100 Hz) involves the heat transfer changes that occur during the engine cycle itself [1]. The peak intra-cycle heat flux in a diesel engine can reach 10–15 MW/m^2 [2,3] and the minimum value is near zero. Analyses of thermal transients in gas turbines [4], which consider only heating or cooling that is on a time scale associated with the low and intermediate frequency ranges mentioned above [4–10], suggest that they play a key role in the degradation of thermal barrier coating systems [5,11].

Research into insulating reciprocating engine surfaces with coatings has been ongoing for almost 45 years. The historical evolution of reciprocating engine thermal barrier coating technology is provided in a recently published literature review [12] that focused on the performance and emission characteristics associated with in-cylinder heat insulation. A discussion of the structural aspects of coatings is rudimentary.

Many of the early coatings applied to the power cylinder components *i.e.*, piston, intake/exhaust valves, cylinder head and liner, were identical of those used in the gas turbine industry. Foundational insights on the subject were generated during the "adiabatic" engine program [13–15], which sought to reduce or even completely remove cooling systems by using high-temperature ceramics. These early coatings were thick, on the order of a millimeter, with "long" thermal conduction time scales that resulted in substantially higher surface temperatures during all strokes of the thermodynamic cycle. The lack of adequate coating design [16,17] led to negligible performance gains, which, in turn, suppressed research in the area.

Abbreviations

rpm	Revolutions per Minute
TDC	Top Dead Center
aTDC	after Top Dead Center
BDC	Bottom Dead Center
IVO	Intake Valve Opening
IVC	Intake Valve Closing
EVC	Exhaust Valve Closing
TBC	Thermal Barrier Coating
YSZ	Yttria Stabilized Zirconia
HCCI	Homogeneous Charge Compression Ignition
ERR	Energy Release Rate
CMAS	Calcium-Magnesium Alumino-Silicates
IMEPg	Gross Indicated Mean Effective Pressure
SOI	Start of Injection
AFR	Air-Fuel Ratio

Researchers [18–20] suggested that thin coatings, on the order of one hundred micrometers, with "short" time scales could *instantaneously* reduce the gas-wall temperature difference that drives convective heat transfer. Such "short" time scales were conceptualized by using thin, highly porous coatings. Toyota Central Research Labs [21–24] designed and demonstrated a thin, low thermal conductivity and low volumetric heat capacity coating for reciprocating internal combustion engine surfaces. The low volumetric heat capacity requirement was achieved via a 100 μm highly porous aluminum structure impregnated with silica [22], termed SiRPA (Silica-Reinforced Porous Anodized Aluminum). This strategy enabled the surface to quickly respond to transient gas temperature fluctuations induced by the combustion event, *i.e.* at the highest frequency discussed above. More specifically, a calculated surface temperature swing during a cycle in excess of 400 °C was predicted for diesel operation [25].

The durability and reliability of such coatings has been the primary issue preventing their widespread implementation. There are multiple reports in the literature of delaminated coatings, spallation, and cracks in the coating following diesel [26–32] and homogeneous charge compression ignition (HCCI) [33] engine testing. Thibblin and Olofsson [32] performed experiments on a heavy-duty diesel engine using a YSZ-coated piston manufactured via suspension plasma-spraying. They performed an SEM analysis of the coating after testing, and reported a unique finding: the coating showed evidence of delamination within the layer, not at the piston–coating interface.

Although structural integrity has been a long-standing problem and many studies have been conducted, limited fundamental work on the mechanics of thermal barrier coating system failure has been performed for reciprocating internal combustion engines. A methodology to predict coating failure at the design stage considering all the aforementioned frequency ranges does not exist. Previous studies have been limited to time-averaged conditions, neglecting the transient intra-cycle temperature fluctuations of the coating [34–37]. Zhu and Miller [38] highlighted the importance of the low and high frequency engine thermal transients for a thick ("long" time scale) YSZ coating. The study presented mechanisms of fatigue crack initiation and propagation as well as creep and fatigue interaction supported by numerical and experimental evidence simulating engine-like conditions. Experiments showed that the combined low- and high-frequency cycle fatigue tests induced more severe coating surface cracking, microspallation and accelerated crack growth than pure low-cycle fatigue tests. Recently, Baldissera and Delprete [39] analyzed the temperature, stress, and displacement distributions of a coated diesel piston. Steady-state thermo-mechanical analysis was performed at a single instant during the cycle, *i.e.* top dead center (TDC). The stress analysis revealed higher peak stresses at the coated surface relative to the uncoated baseline.

Existing approaches to durability of reciprocating engine coatings have been predominantly stress-based [40–43]. However, because the coatings are loaded with pre-existing microcracks and flaws, delamination and spalling is not controlled by crack initiation events (which might be susceptible to a stress-based analysis). Rather, it is controlled by conditions were an initiated crack can advance multiple coating thicknesses (*e.g.*, delamination). Fracture-based approaches are more appropriate to assess the durability of coatings and its sensitivity to design parameters however, they are non-existent to the authors' knowledge.

The objective of this work is to develop a framework for predicting coating failure in reciprocating internal combustion engines that combines a rigorous analysis of thermal transients during an engine cycle with a thermomechanical analysis of coating stress and the driving forces for delamination. The highly transient nature of the heat flux in reciprocating engines requires many computations to be evaluated. High computational efficiency was achieved through an analytical treatment of the mechanics following Begley and Hutchinson [44]; energy release rates were computed assuming equi-biaxial stress followed by plane strain delamination. The results reveal unique insights into when in the cycle and where in the coating failure is expected for reciprocating engines.

The analysis was performed for the geometry shown in Fig. 1 relevant to steady-state edge delamination which for clarity shows just a single coating layer applied to a flat substrate having uniform thickness (the engine piston in this case). The combustion chamber lies above the coating which is thin compared to the substrate which is cooled on its bottom surface. Distributions of the

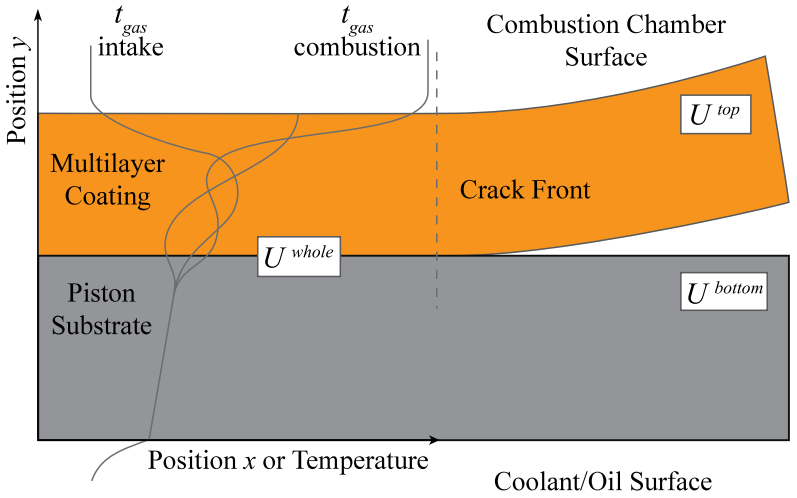

Fig. 1. Schematic illustration of a thermal barrier coated piston exposed to combustion chamber gases (top) and coolant/oil (bottom). On the left side the intact (whole) wall temperature distribution is illustrated at three times during the cycle, *i.e.* intake, combustion, and mid-expansion. The right side depicts a delamination scenario where the energy release rate G overcomes the toughness and cracking occurs. The stored elastic strain energy of the intact structure and for the upper and lower parts behind the crack, indicated as U^{whole}, U^{top} and U^{bottom}, are used to calculate the energy release rate as given in Eq. (B.20).

temperature, t, through the layered system are sketched in the figure (with the higher temperature to the right). At a time during the intake stroke the gas temperature is low (~350 K) and heat flows from the coating/substrate multilayer into the gas. At a time during the combustion event the gas temperature is high (~2500 K) and the heat flows from the gas into the multilayer. Depending on the coating properties, the temperature at the top surface ($y = 0$) can vary several hundred degrees Kelvin during a cycle. A temperature distribution at an intermediate time during the expansion stroke is also illustrated. In an actual engine the coating temperature varies significantly both temporarily and spatially, *i.e.*, $t = t(\theta, x, y)$, while the substrate temperature has a relatively weak variation in time but varies spatially. In this paper, the focus will be on the temperature variations in the hottest regions experienced by the multilayer, and thus we idealize the problem by restricting consideration to temperature variations that are dependent only on time and the coordinate normal to the interfaces, $t = t(\theta, y)$.

As it will be seen in the results to follow, the coating stresses driving delamination failures of the intact coating are equibiaxial compression, *i.e.*, $\sigma_y = \sigma_z < 0$. Two types of delamination can occur under compression: edge delamination and buckling delamination. Both types require initial flaws in the coating or coating/substrate interface to trigger delamination, but for thin systems the size of these flaws need only to be quite small, typically on the order of the coating thickness for edge delamination. For edge delamination, the flaw can be a small crack in the coating or on the interface at an actual edge. The flaw could also be located at through-crack or gap in an interior region of the coating. For buckling delamination, a crack-like flaw parallel to the interface is required, either within the coating or on the interface, large enough to initiate local buckling of the portion of the coating above the flaw. Both types of delamination are driven by the elastic energy per area in the coating at the instant in question. For the simplest example in which the stress in the coating is uniform and delamination occurs at the interface, the energy per area in the coating, U, is proportional to $\sigma_x^2 L/E$, where L is the coating thickness and E is its Young's modulus. The precise result for the energy release rate of a steady-state edge crack delaminating under plane strain conditions for the uniformly stressed coating is $G = \sigma_x^2 L/(2\bar{E})$, independent of σ_z, where $\bar{E} = E/(1-\nu^2)$. The condition for growth of the delamination is $G = G_c$, where G_c is the toughness (measured in energy/area, Jm^{-2}) of the coating or interface depending on the location of the delamination crack. To attain steady-state the edge crack must have advanced on the order of several times L, depending on where it originates [44]. Once steady-state conditions are attained, G remains at the steady-state value. The special relevance of steady-state delamination is that, if the stress and crack length for this condition are attained or exceeded (*i.e.*, $G \geq G_c$), large patches of the coating will fail. With uniform compressive stress in the coating and separation at the interface, the energy release rate at each crack tip of a buckle delamination is $G = f\sigma_x^2 L/(2\bar{E})$, where the factor f increases as the buckle spreads, approaching unity, if it is straight-sided. Thus, a sufficiently large straight-sided buckle delamination has the same energy release rate as the edge crack. The factor f approaches a limit that is slightly different from unity, depending on Poisson ratio, ν, if the delamination is circular [44]. The edge crack has mode II conditions at the crack tip, while the buckling delamination tip is mixed mode but becomes increasingly mode II as it spreads.

In this paper, to reveal the essence of conditions driving delamination of coatings on the piston surface of a compression ignition diesel engine, we will compute and present results for the steady-state energy release rate of an edge crack as dependent on the coating properties and engine running conditions. The steady-state energy release rate combined with the criterion, $G < G_c$, ensures that large patches of delamination will not occur. Based on the above discussion, the steady-state edge crack results will pertain as well to the crack driving force for buckle delamination, at least approximately. It is also evident from the above discussion that the toughness, G_c, controlling spread of the delamination should be the mode II toughness, at least approximately. If the

Table 1
Single cylinder research engine operating conditions under investigation [48] .

Condition	Speed [rpm]	IMEPg [bar]	AFR [–]	SOI [°aTDC]	Injection duration [°]
50% Load	1700	12.3	29	−22	10.7
Rated Power	2500	20.3	26.8	−29	21.6
Combat Rated Power	2750	29.7	25.5	−9	40.5

IMEPg: Gross Indicated Mean Effective Pressure; AFR: Air-Fuel Ratio; SOI: Start of Injection.

fracture-based approach to coating delamination in this application proves promising, more detailed analyses will almost certainly be warranted. These could include studies of the initiation process when delamination cracks first emerge from flaws in the coating or at the interface, and investigations of the competition between edge-type delamination and buckle delamination. It should be noted however that experience with many other thin film and coating systems has suggested that the condition, $G < G_c$, based on the steady-state energy release rate, G, is not overly conservative, most probably due to the fact that thin films and coatings cover vast area compared to their thickness providing ample opportunities for flaws.

2. Thermal model

One-dimensional transient heat transfer is assumed through the coating and substrate. Conventional diesel combustion has considerable in-cylinder heat flux spatial discrepancy [45], however, the focus of the heterogeneous surface temperature distribution was outside of the scope of this work. Such problem can be practically dealt with by adding an appropriate safety factor to the applied spatially averaged heat flux. An unsteady heat flux (described below) was used as the boundary condition on the combustion chamber surface side of the domain, and a steady temperature of 100 °C was assumed at the piston underside. A Crank–Nicolson numerical scheme was used to integrate the unsteady, one-dimensional heat diffusion equation [46,47] The spatial domains, *i.e.* the piston substrate and the coating, were linearly discretized with 2^5 and 2^7 nodes, respectively. Further details about the finite difference convergence criteria can be found in Koutsakis et al. [47].

The combustion chamber heat flux that drives the thermal model was taken from the literature. Gingrich et al. [3] used a wireless piston telemetry system to acquire fast-response surface temperature data from which heat flux was estimated via Fourier decomposition analysis. Fifteen discrete piston thermocouple locations were measured, and the spatially integrated, area-weighted heat flux that represents the total in-cylinder heat transfer [3,48] was utilized in the present work. A wide range of operating conditions were explored by Gingrich et al. [48], including some very high output conditions. Three engine conditions were selected for study based on medium, high and very high power output. Details of the operating conditions are given in Table 1. The most advanced start of injection (SOI) for each condition, which is the most thermally severe [3], was selected to evaluate coatings' structural integrity.

The area-weighted heat fluxes for these operating conditions are shown in Fig. 2 as a function of time. The heat flux data have different durations since they were acquired at different engine speeds. Following the convention of reciprocating engine analysis, all of the following data will be presented using crank angle as the time axis; the compression stroke begins at −180°, and top dead center (minimum volume) for combustion occurs at 0°. The 50% Load case has a peak heat flux of 5 MW/m^2, which is typical of a light-to-medium duty commercial vehicle. The nearly 12 MW/m^2 area-weighted peak heat flux of the Rated Power condition is quite high for medium- and heavy-duty engines. It is worth noting that the Combat Rated Power condition, which represents a condition of maximum power that can be achieved for short duration, has a peak heat flux almost 2.5× lower than the Rated Power condition. The cause for this behavior is the extended ignition duration and late combustion phasing to avoid mechanical failure [3], see Table 1.

3. Delamination model

The impact of the thermal transients on coating mechanics is analyzed using well-established techniques [44]. The temperature profiles obtained in the previous section are used as inputs to compute the local thermal stresses and strain energy density in the multilayer at each point in time. The presented analysis ignores the fact that the delamination crack at the interface may impede the heat flow through the interface region in the manner considered and thereby change the temperature distribution near the crack tip and in the delaminated region. In turn, this change in the temperature distribution may alter the energy release rate. However, if the delamination crack advances rapidly, as would be expected if the energy release rate exceeds the toughness, there would not be time for thermal redistribution to take place, and the results derived would be valid. There are scenarios in which the change in temperature distribution due to the separation caused by the delamination might have some influence on the energy release rate, and these might be worth investigating in subsequent work. Both the coating and the substrate are assumed to be isotropic, elastic layers that experience stretching in the plane of the layers and bending about the in-plane axes. Durability is assessed in terms of the energy release rate for delamination cracks that run parallel to the coating; given the transient nature of the temperature distribution, the driving force for cracks at arbitrary depths relative to the surface and all times are considered. Full details of the analysis are available in the appendix and largely follow those in [9,44].

For layers whose in-plane dimensions greatly exceed their thickness, the total strain in both layers can be approximated as $\epsilon(y) = \epsilon_o - \kappa \cdot y$, where y is the position measured from the bottom of the substrate. Here, ϵ_o denotes the stretch of the bottom axis of

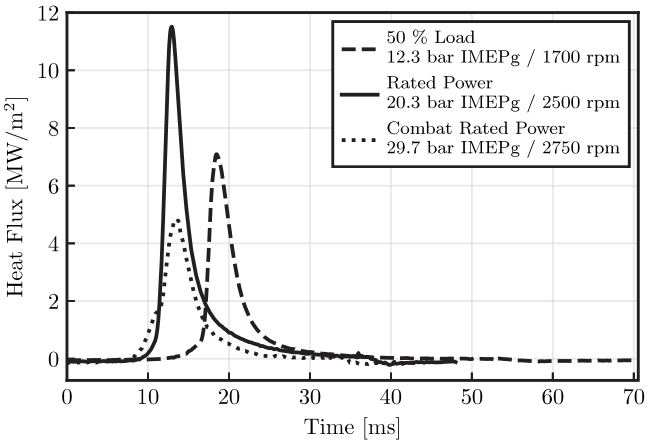

Fig. 2. Experimental area-weighted heat fluxes obtained via telemetry measurements on an uncoated-piston. Details of the engine operating conditions can be found in Table 1.

the layer, while κ denotes the curvature of the layer that induces bending strains. The stretch and curvature are evaluated from the resultant moment and force at each time, as will be evident below. As will be demonstrated, these bending strains are negligible for the present cases that involve relatively stiff, thick substrates. The above kinematics applies to both the substrate and the coating; however, bonded and debonded sections have different stretch and curvatures due to differences in in-plane stresses. To compute the strain energy in the system, one must compute the stretch and curvatures for each section, *i.e.* the intact region, and regions above and below the delamination plane, and the associated strain energies. In all regions of the bilayer, the stress normal to the interface σ_y and shear stresses are assume to be negligible.

Here, we assume that cracking relieves the in-plane stress in the layer above the delamination crack, but does not change of the out of plane deformation. This corresponds to the following relations for total strain components:

$$\text{Intact section:}\quad \epsilon_x = \epsilon_z = \epsilon_o^i - \kappa^i y \tag{1}$$

$$\text{Above the crack:}\quad \epsilon_z = \epsilon_o^i - \kappa^i \cdot y$$

$$\epsilon_x = \epsilon_o^{top} - \kappa^{top} y \tag{2}$$

$$\text{Below the crack:}\quad \epsilon_z = \epsilon_o^i - \kappa^i \cdot y$$

$$\epsilon_x = \epsilon_o^{\text{bot}} - \kappa^{\text{bot}} y \tag{3}$$

where ϵ_o^i and κ^i are the stretch and curvature of the intact section of the bilayer respectively, and ϵ_o^{top} and κ^{top} are the stretch and curvature of the layer above the delamination respectively; ϵ^{bot} and κ^{bot} are the stretch and curvature of the layers below the delamination plane, respectively, which is a bilayer provided the crack location is not at the interface.

For each section, the unknown stretch and curvature can be computed from the resultant moment and force acting on the bilayer; in the present analysis, we assume reaction forces/moments due to constraint of the substrate edges is negligible, such that $M = \int_{\text{bot}}^{\text{top}} \sigma_x(y) y dy = 0$, and $N = \int_{\text{bot}}^{\text{top}} \sigma_x(y) dy = 0$. Using the above kinematics and the thermoelastic constitutive law $\epsilon_x = \sigma_x/E - \upsilon\sigma_z/E + \alpha\left[t(y) - t_{\text{ref}}\right]$ (and similarly for ϵ_z), where α is the coefficient of thermal expansion, one obtains two algebraic equations for the two unknowns, *i.e.* ϵ_o and κ. These integrals can be conveniently performed on a piece-wise basis using the numerical grid of the temperature analysis; the crack can be placed at any point on the grid, with the above kinematics applied in corresponding layers. Complete details of the stretch and curvature computation are provided in Appendix.

Literature information related to the stress-free temperature of coatings for reciprocating engines were not available. The reference temperature was taken as the mean surface temperature measured during the plasma spray deposition [49]. The effect of different residual stresses is discussed below. In this work, it was assumed that the coatings do not undergo creep relaxation during operation.

The strain energy released during delamination defines the energy release rate for a delamination crack; for a crack length that is much longer than layer thickness, the 'steady-state' energy release rate is at its maximum and is independent of crack length. This steady-state energy release rate is given by:

$$G = U^i - \left(U^{\text{top}} + U^{\text{bottom}}\right) \tag{4}$$

where U^i is the strain energy per unit length in the intact section of the bilayer, while U^{top} and U^{bot} are the strain energies per unit length in the two sections formed by the delamination crack. In terms of stresses, the strain energy is given by:

$$U = \int_{y_{\min}}^{y_{\max}} \left[\frac{1+\upsilon}{2E}\left(\sigma_x^2 + \sigma_z^2\right) - \frac{\upsilon}{2E}\left(\sigma_x + \sigma_z\right)^2\right] dy \tag{5}$$

Table 2
Thermo-mechanical properties of wall architectures investigated, with k: thermal conductivity; ρ: density; c: specific heat capacity; L: thickness; E: Young's modulus; α: coefficient of thermal expansion; and ν: Poisson ratio.

Material	k [W/m-K]	ρ [kg/m^3]	c [J/kg-K]	L [μm]	E [GPa]	α [ppm K^{-1}]	ν [–]
YSZ [49,50]	0.77	4713	388	200	41	12	0.2
Cordierite-YSZ [49,51]	0.37	2855	347	200	18	6.8	0.25
Steel 4140 Piston [52,53]	39	7850	520	4800	180	13.5	0.29

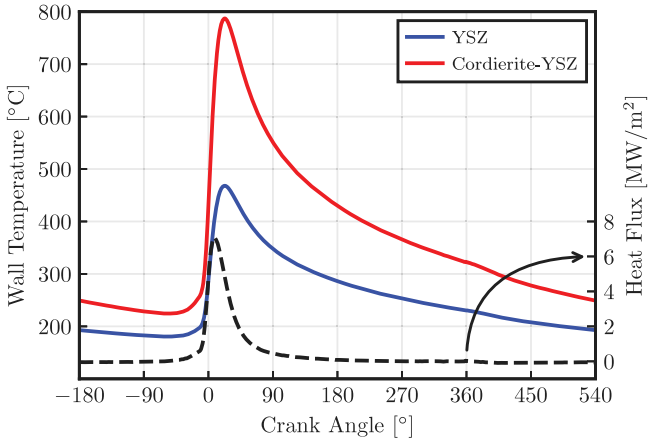

Fig. 3. Surface temperature (solid lines, left axis) evolution as a function of crank angle for a YSZ (blue) and a Cordierite-YSZ (red) coating. Both coatings have 200 μm thickness. The applied heat flux is shown on the right axis. Note, the cycle shown corresponds to a total time of 48 ms.

where the integral of the strain energy density takes into account position-dependent stresses that arise from position-dependent properties, temperatures, per the thermal model, and different stretch and curvature values for each section. Delamination is expected when G exceeds the corresponding material toughness at the location of the crack, G_c. In the present study, the additional complication of a mode-dependent toughness is neglected; see [9,44] for a treatment of these effects.

The analytical relationship found in the Appendix offers significant computational advantages as compared to other numerical integration approaches [44]. Computational efficiency is particularly important for establishing energy release rate calculations in the unsteady environment of internal combustion engines. In practice, several hundred energy release rate evaluations are required per each engine cycle. For this study, the energy release rate was calculated every 1 crank angle, *i.e.* 720 evaluations for every thermodynamic cycle.

4. Results and discussion

Two thermal barrier coatings from the modern engine literature were selected for investigation. The first was yttria-stabilized zirconia, YSZ, a traditional engine coating [50] and the second was Cordierite-YSZ, a novel low thermal conductivity, low volumetric heat capacity coating [51]. Detailed coating property data can be found in Table 2. The thermal properties for these coatings are provided in the references; the mechanical properties of both coatings were provided by the Thermal Spray Lab of Stony Brook University [49]. The piston substrate was 4140 steel, which is often used in heavy-duty applications [52,53]. The coating thickness was fixed (200 μm) except for in the section below where it was parametrically varied. The term *wall* is used to define the intact multilayer, *i.e.* bonded coating and substrate, unless otherwise specified.

The surface temperature behavior as a function of piston position is illustrated for the 50% Load case in Fig. 3. The heat flux profile from Fig. 2 is superposed to illustrate the phasing difference between the heat flux and temperature profiles. The YSZ (blue) and Cordierite-YSZ (red) coatings provide a surface temperature swing of 290 °C and 560 °C, respectively. One may expect the Cordierite-YSZ coating to increase engine thermal efficiency due to the higher temperature swing, which would give less heat transfer during the expansion stroke, but the higher surface temperature during the intake stroke may have a negative impact on engine breathing [25].

4.1. Engine cycle histories

The coupled analysis is demonstrated for the Rated Power engine condition and the YSZ coating in Fig. 4. The results shown in Figs. 4 and 5 (discussed below) are typical of all the cases considered. Only the 360 crank angle degrees of the engine cycle during compression and combustion, where most of the changes take place, are shown in Fig. 4. This time period corresponds with the heat flux impulse shown in (a), for reference also see Fig. 2. The temperature histories at four discrete locations are shown in

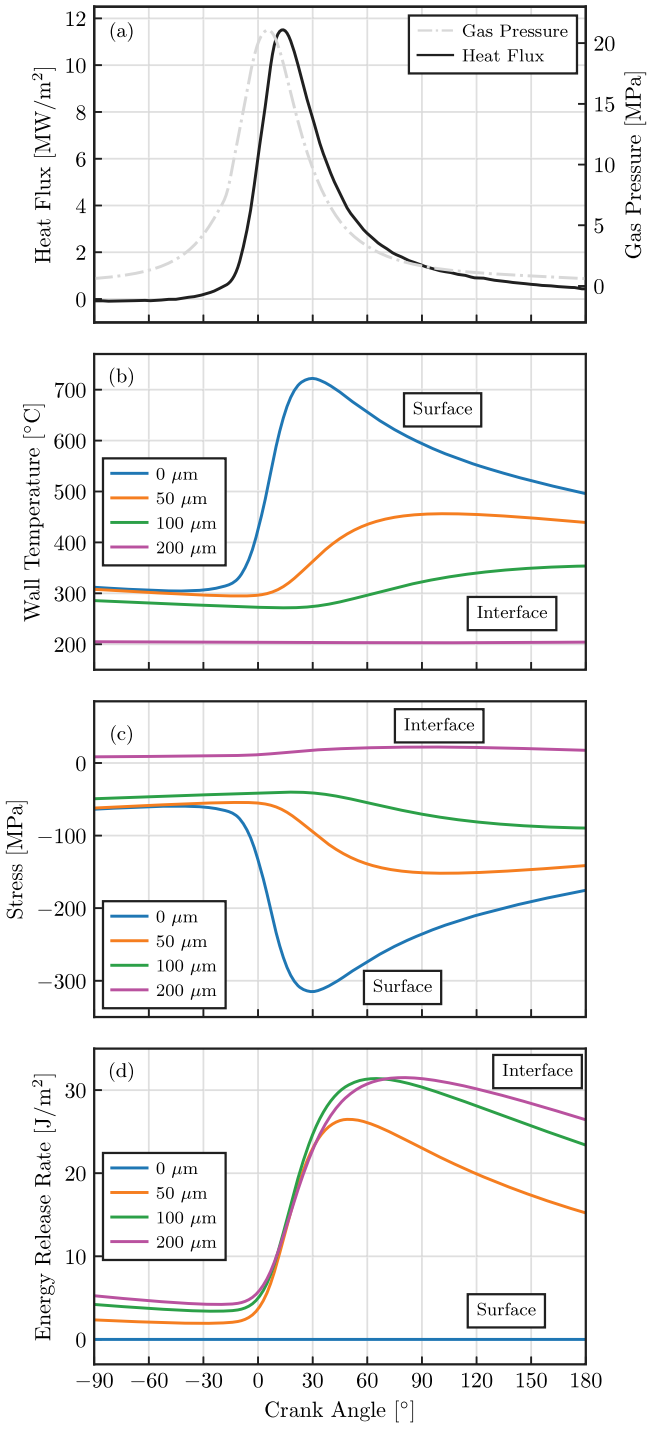

Fig. 4. Crank resolved evolution combustion chamber cylinder pressure (gray) and heat flux (black) (a), wall temperature distribution (b), x-direction stress distribution (c) and elastic energy release rate distribution (d) are shown during an engine cycle for the Rated Power condition. The surface (blue), 50 μm (orange), 100 μm (green) and interface 200 μm (pink) is depicted on (b), (c) and (d). Stress-free temperature and coating thickness was held constant at 230 °C and 200 μm, respectively. The Rated Power engine condition specifications and the thermomechanical properties of YSZ/Steel can be found in Table 1 and 2, respectively.

Fig. 4(b). The coating surface ($y = 0$) temperature follows the rapid increase of heat flux up to its peak value at 30°aTDC, but the temperature decays much slower than the heat flux. The amount of intra-cycle temperature change reduces progressing deeper into

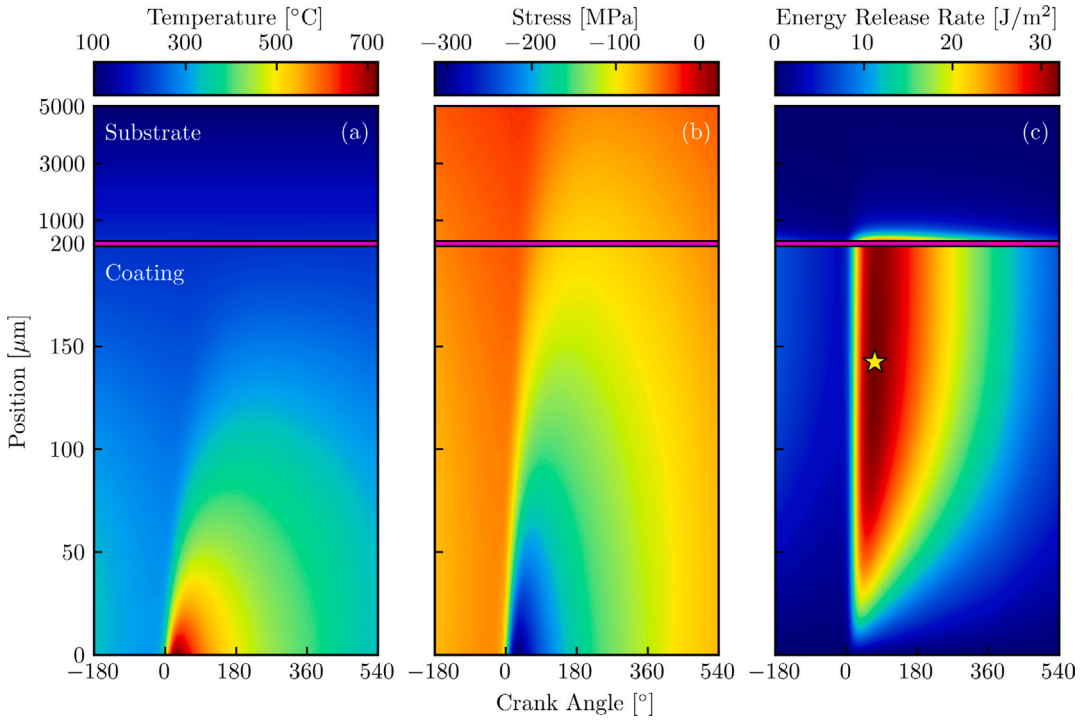

Fig. 5. Spatial and temporal (in crank angle domain) evolution of temperature (a), stress (b) and energy release rate (c) using a YSZ thermal barrier coating on top of a piston substrate of an internal combustion engine cycle for the Rated Power condition. Combustion chamber surface and oil surface is at $y = 0$ and $y = 5000$, respectively. Coating–piston interface is indicated with the horizontal pink at 200 μm. The stress-free temperature was at 230 °C. Wall architecture and operating condition was equivalent to Fig. 4.

the wall; *e.g.* the coating–piston interface temperature varies by less than 4 K. The intra-cycle temperature variations in the piston substrate are negligible.

The stress histories at the same through-thickness locations are shown in Fig. 4(c). Negative and positive values indicate compressive and tensile stress, respectively. The vast majority of the thermal barrier coating is under compression; in this case, the reference temperature was set at 230 °C [49]. As the surface temperature is increasing due to combustion, the compressive stresses in the coating increases. The maximum stress in the wall is observed to be exactly when and where the temperature distribution is maximized, *i.e.*, 30°aTDC at the surface.

The energy release rate, G, as a function of engine crank-angle (time) is shown in Fig. 4(d). Immediately after the start of combustion, the energy release rate increases due to heating of the coating surface. The energy release rate histories show that the peak driving force for delamination occurs later in the cycle, around 60°aTDC, past the instant in time where the surface temperature and stress in the coating are at their maxima.

At a peak cylinder pressure of 25 MPa the compressive stress is about 10% of the maximum stress seen at the surface. However, the time at delamination (peak energy release rate time) in question occurs later in the cycle. There is a significant delay between the peak pressure (stress) and peak energy release rate — at least 30°. At the time of peak energy release rate in the expansion stroke (about 60°aTDC), the cylinder pressure is reduced to about 2 MPa, which is considered negligible compared to the compressive stresses generated due to thermal loading (about 250 MPa at 70°aTDC).

Fig. 4 shows only four spatial locations for clarity. In reality, since the maximum energy release rate occurs at an unknown time and location, it needs to be computed at all times and locations. These data are shown in Fig. 5, which provides a more comprehensive view of the temperature, stress and energy release rate distributions throughout the coating and engine cycle. The engine conditions are the same as Fig. 4. The horizontal and vertical axes represent crank-angle (time) and position through the wall, respectively. The latter has two different linear scales: 0-200 μm for the coating, and 200-5000 μm, for the substrate. The coating–substrate interface lies on the horizontal pink line, at 200 μm. The contour maps in Fig. 5 are broadly representative of all cases considered in this work. Fig. 5 makes it easy to see the penetration of the thermal (and corresponding quasi-steady stress) profile into the coating, and the resulting evolution of the energy release rate distribution.

The maximum energy release rate, highlighted with the yellow star, occurs during the expansion stroke, at 72°aTDC at a depth of 142 μm. At this time of the cycle, the surface of the coating is cooling but the interior region is still heating. It is interesting to note that the position of the maximum energy release rate is near the mid-coating region. This behavior suggests that, for cases where energy release rate exceeds the toughness, the coating would have higher likelihood to crack at the mid-coating area than at the coating–substrate interface. This is a unique feature brought on by the cyclic thermal loading of the engine, and is discussed more below.

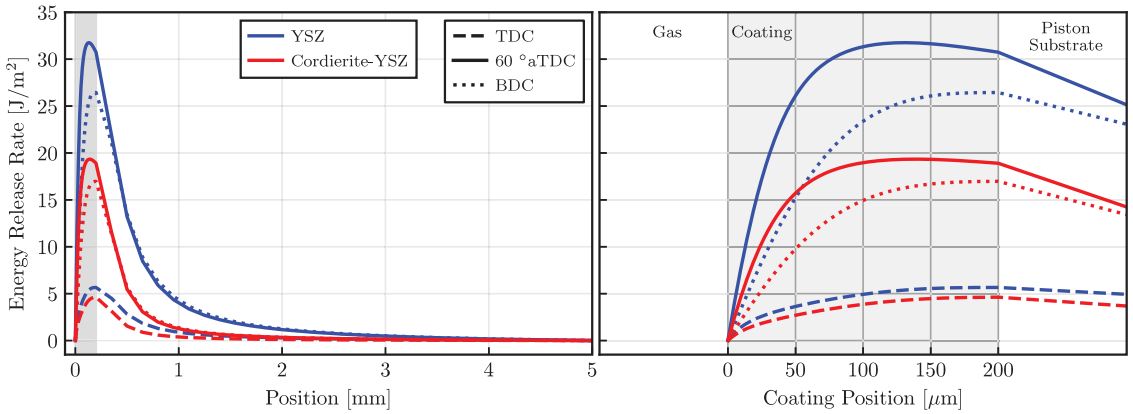

Fig. 6. (a) Energy release rate spatial distribution is shown for the entire engine wall, *i.e.* coating and substrate. Two different coatings and three distinct crank angle locations are illustrated. The shaded area highlights the coating YSZ (blue) and Cordierite-YSZ (red) coating. The results shown are at TDC (dashed), 60°aTDC (solid) and BDC (dotted). The same engine condition as Figs. 4 and 5 were used. The stress-free temperature was 230 °C. Thermomechanical properties can be found in Table 2. (b) Expanded version of the energy release rate spatial distribution in the coating.

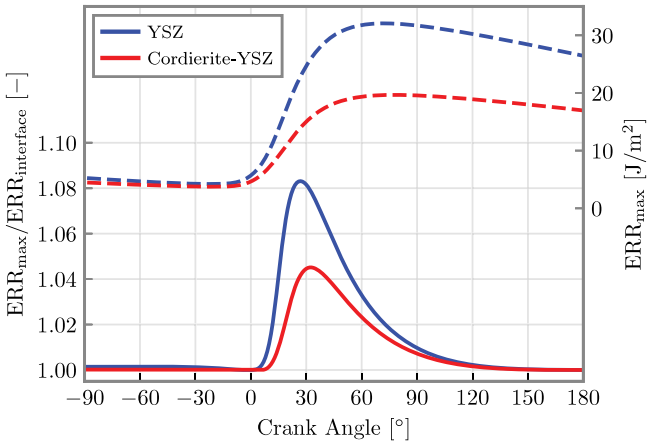

Fig. 7. Ratio between maximum and interface energy release rate (left axis) and maximum energy release rate (right axis) during the compression and expansion stroke for the YSZ and Cordierite-YSZ coatings.

4.2. Effect of coating material

A comparison of the spatial distribution (normal to the wall) of the energy release rate for the two different coating materials at the Rate Power condition is shown in Fig. 6. The full domain is shown at the left, and a magnified view of the coating is shown at the right. The shaded region ranging from 0 to 200 μm corresponds to the coating material, with the combustion chamber gas (heat flux input) to the left. Results are shown for three distinct times in the cycle, denoted by line style, and both coatings, denoted by color. Both coatings had a fixed stress-free temperature of 230 °C. The two coatings follow a very similar pattern, but the energy release rate for the YSZ coating is higher in magnitude at all times. The Cordierite-YSZ coating has lower thermal conductivity and volumetric heat capacity, and therefore experiences a higher temperature swing and higher peak temperature in the cycle than the YSZ, which would suggest higher energy release rates. However, the higher coefficient of thermal expansion and Young's modulus of the YSZ outweigh the more severe thermal environment for Cordierite-YSZ, resulting in the observed trend.

In Fig. 5 it was shown that the maximum energy release rate was found within the coating, not at the interface. This effect is seen to occur for both coating materials in Fig. 7, which depicts the data on a temporal basis. The maximum energy release rate, shown on the right axis, is seen to peak at the same crank angle for both coatings. The ratio of the maximum energy release rate at a given time to the corresponding value at the coating–substrate interface is shown on the left axis of Fig. 7. The times of most interest are those with high energy release rate, *i.e.* after top dead center. It can be seen that during this period the maximum value exceeds the interface value by up to 8%, and is about half of that magnitude at the time of peak energy release rate. The data in Fig. 6 confirm that the maximum value lies within the coating. Qualitatively, this result agrees with the findings of Thibblin and Olofsson [32].

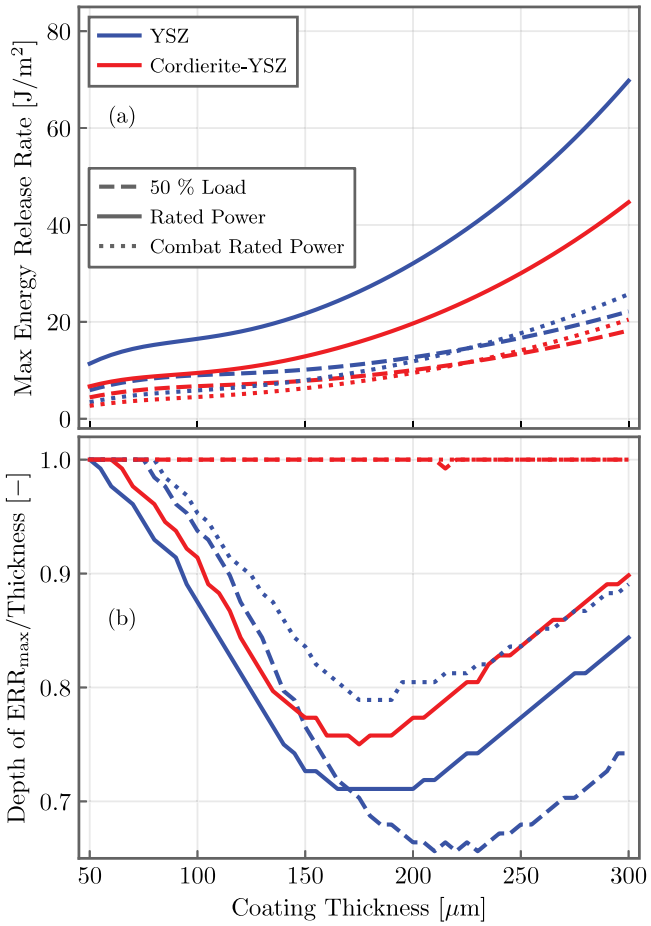

Fig. 8. Effect of increasing coating thickness on (a) the maximum energy release rate, and (b) the ratio between the depth of maximum energy release rate and coating thickness. Engine conditions details for the 50% Load (dashed), Rated Power (solid) and Combat Rated Power (dotted) can be found in Table 1. Thermomechanical properties of the YSZ (blue) and the Cordierite-YSZ (red) coating can be found in Table 2. The stress-free temperature was 230 °C.

4.3. Effect of coating thickness

The thickness is a critical parameter that controls coating performance. A thicker thermal barrier coating reduces heat transfer, but may have deleterious effects on overall engine performance and coating durability. The energy release rate of a gas-turbine coating, assuming a heating or cooling scenario, scales linearly with thickness [8,44]. There are a few fundamental differences between a coated piston and a coated gas turbine blade. The first is the time scale of the transient processes. Second, the backside temperature for the piston is considered constant during an engine cycle, but for the turbine blade it may change substantially during a take-off or landing thermal transient.

Fig. 8(a) shows the effect of the coating thickness, ranging from 50 μm to 300 μm, on the maximum energy release rate during a cycle for all three engine operating conditions, denoted by line style, and both coatings, denoted by color. The peak energy release rate is seen to increase with coating thickness, as expected, but in a nonlinear manner. The nonlinear dependence is driven by the transient heat flux conditions. The highest peak energy release rates were observed for the Rated Power condition, which has the highest heat flux, see Fig. 2. The other two engine conditions, which had comparable peak heat flux, behaved similarly to each other.

The magnitude of the maximum energy release rate, however, does not encapsulate all of the coating thickness effects. Fig. 8(b) shows the ratio of the depth of the maximum energy release rate to the coating thickness as a function of the coating thickness; a value of unity indicates that the maximum energy release rate is at the piston-coating interface. For the Cordierite-YSZ coating, the maximum energy release rate was at the interface for both the 50% Load and Combat Rated Power conditions, while for YSZ the maximum value was found within the coating for all three cases. For cases where the ratio was less than unity, *i.e.,* the maximum occurs in the coating, the location is dependent on the coating thickness. As the coating thickness increases up to around 200 μm, the location of the maximum energy release rate moves further into the coating. This suggests that thicker coatings may be prone to ablate as compared to peel. For thickness greater than 200 μm, the location of the maximum energy release rate moves towards the interface.

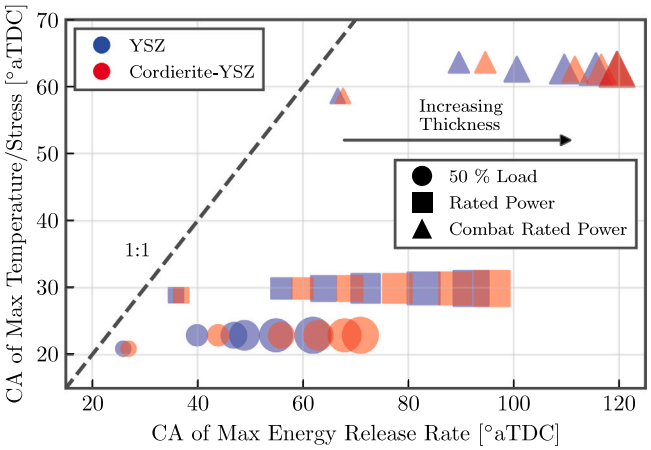

Fig. 9. Comparison of crank angle location of maximum surface temperature or stress to the crank angle location of maximum energy release rate observed in a cycle. Every point lies below the 1:1 line, indicating that the energy release rate maximum occurs later in the cycle than the maximum of temperature or stress. The marker size indicates increasing coating thickness from 50 μm to 300 μm.

The maximum energy release rate is also found at different times during the engine cycle as coating thickness changes. Fig. 9 shows the relationship between the crank angle location of the maximum surface temperature to the corresponding value of maximum energy release rate. The coating thickness is represented by the size of the marker and corresponds to the range of values used in Fig. 8. The time of maximum energy release rate is seen to always lag the time of peak surface temperature or stress maximum, *i.e.*, lie below the 1:1 line. The maximum energy release rate may occur anywhere between 5 to almost 60°aTDC later in the expansion stroke than the maximum temperature.

4.4. Effect of deposition (residual) stresses

The majority of aircraft engine coating studies [44] assume that the stress-free temperature is the highest steady-state temperature that the coating experiences when exposed to combustion gases, *i.e.* $t_{\text{wall}} \geq 1300$ °C at the surface. The rationale is that at such high temperatures the coatings will relax and creep. This is not valid for reciprocating engine operation, however. Even under the most extreme conditions (analogous to the current Rated Power case), the maximum temperature of the coating is held for only a couple of milliseconds, and the peak temperature is localized at the surface. The inner part of the wall/coating experiences lower temperatures. Therefore, the stress-free temperature is not dominated by the combustion gas temperature. It is more likely that the stress-free state is defined by the temperature that the substrate was preheated to prior to and during coating deposition. This process-related temperature may be an important design parameter for thermal barrier coatings in reciprocating engines.

Fig. 10 shows the effect of the reference temperature on the maximum energy release rate during a cycle for all three engine conditions and both coatings. The reference temperature range, from 100 to 350 °C, was chosen to be representative of plasma spray deposition techniques. The coating thickness was held fixed at 200 μm. For increasing reference temperature the maximum energy release rate in the cycle is increased. Generally, higher reference temperature results in higher compressive stress, and thus strain energy at room temperature. For engine operation, the reference temperature adds an extra compressive stress component to the total compressive stress, as can be observed from Eqs. (B.1) and (B.5). As a practical example, for the Cordierite-YSZ coating the results suggest that the maximum energy release rate can be reduced 3× simply by decreasing the reference temperature from 350 °C to 100 °C.

Recall, this stress-free temperature does not alter the heat transfer physics of the problem, and it can be modified by the manufacturing process.

5. Summary and conclusions

Failure analysis of thin thermal barrier coatings for reciprocating engines was performed using a coupled thermomechanical approach. An analytical method to evaluate transient energy release rate assuming equi-biaxial stress followed by plane strain after delamination was utilized. The highly unsteady nature of the applied heat flux and resulting thermal wave in the solid require evaluation at all times in the engine cycle to determine when and where the peak energy release rate is likely to occur. A transient finite difference solution of the 1-D heat diffusion equation was used to determine the temperature distribution. The method was demonstrated for two thermal barrier coatings and high output diesel engine operating conditions.

The proposed approach to analyze durability of reciprocating engine coatings was fracture-based as compared to other stress-based approaches. The key results from this analysis are:

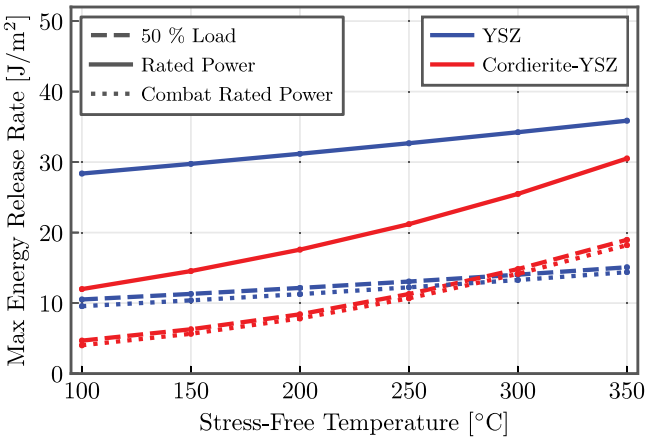

Fig. 10. Effect of stress-free/reference temperature (ranging from 100 to 350 °C) on maximum energy release rate observed in a cycle for different engine conditions and coating architectures. The coating thickness remained fixed at 200 μm. Engine conditions details for the 50% Load (dashed), Rated Power (solid) and Combat Rated Power (dotted) can be found in Table 1. Thermomechanical properties of the YSZ (blue) and the Cordierite-YSZ (red) coating can be found in Table 2.

- The peak energy release rate was found to occur at a time in the expansion stroke significantly later than the time that the peak surface temperature and stress were observed. At this time the surface is cooling, but a significant fraction of the coating is still undergoing heating.
- The peak energy release rate did not always coincide with the coating–substrate interface. Under the most severe thermal conditions (highest peak heat flux) the location was found to lie within the coating. This suggests that the coating may begin to fail via spalling rather than pealing off the substrate.
- The peak energy release rate was found to scale directly with coating thickness, but in a nonlinear manner. This was a result of the unsteady nature of the applied heat flux.
- The location of peak energy release rate within the coating was found to vary with coating thickness in a non-monotonic fashion. The time in the cycle of peak energy release rate was found monotonically increase with coating thickness, which is consistent with the longer time for thermal penetration.
- The magnitude of the peak energy release rate was found to depend on the stress-free temperature, which is a manufacturing process variable; for engine applications there is not a significant amount of time spent at high temperatures, unlike in gas turbine applications where creep dominates and the reference temperature is governed by operating temperatures.

CRediT authorship contribution statement

G. Koutsakis: Writing – original draft, Validation, Software, Conceptualization. **M.R. Begley:** Writing – review & editing, Validation. **J.W. Hutchinson:** Writing – review & editing, Supervision, Conceptualization. **J.B. Ghandhi:** Writing – review & editing, Supervision, Resources, Funding acquisition, Conceptualization.

Declaration of competing interest

The authors declare that they have no known competing financial interests or personal relationships that could have appeared to influence the work reported in this paper.

Acknowledgments

The authors are grateful to the following colleagues for their technical contributions and insights in support of this effort: Eric Gingrich and Mike Tess (U.S. Army Combat Capabilities Development Command, Ground Vehicle Systems Center, Warren, MI), John Saputo and Sanjay Sampath (both from Stony Brook University, NY). This work was supported by the Deere & Company.

Appendix A. Experimental setup

Experimental heat transfer data from an AVL 530 single-cylinder research engine at the U.S. Army Ground Vehicles Systems Center were utilized as the input for this work [3]. The engine was modified for high-power output diesel operation and is rated for 107 kW at 2750 rpm. Detailed engine geometric specifications can be found in Table A.3. The engine peripherals, *i.e.*, intake, exhaust, coolant, oil and fuel subsystems, were instrumented and the exhaust composition was measured to allow *global* thermodynamic

Table A.3
Single-cylinder research engine geometric specifications [48].

Displacement [L]	1.49
Bore [mm]	122
Stroke [mm]	128
Connecting Rod Length [mm]	239
Number of Valves [–]	4
IVO [°aTDC]	−354
IVC [°aTDC]	−158
EVC [°aTDC]	346
Swirl Ratio [–]	1.3

IVO: Intake Valve Opening, IVC: Intake Valve Closing, EVC: Exhaust Valve Closing.

Table B.4
Effective moduli and misfit strain coefficients prior and during the delamination process.

Mechanics process	Pre-delamination	Delamination
State of deformation/stress	Equi-biaxial	Plane strain
Effective modulus, $\bar{E}$	$E/(1-\nu)$	$E/\left(1-\nu^2\right)$
ϑ coefficient, $\bar{c}$	1	$1+\nu$

measurements to be performed and compared with the *local*, high-bandwidth in-cylinder heat flux measurements. The consistency between these two data sets provides confidence in the measured experimental heat flux [3,48].

A wireless piston telemetry system was used to acquire fast-response surface temperature data at fifteen radial locations; the microwave-based telemetry system has an advertised bandwidth of 10 kHz. The thermocouples were coaxial, J-type surface thermocouples with a mix of plated and sliver junctions depending on the piston curvature. The surface temperature data were ensemble averaged, then low-pass filtered at 2 kHz before the Fourier decomposition method was used to recover heat flux. Heat flux data were acquired using three injector clocking positions, and the results were interpolated to find the spatial heat flux distribution for a sector of the piston corresponding to one injector plume. The data were then integrated (spatially) to find a global heat transfer that represents the total in-cylinder heat transfer, and finally normalized by the piston sector area to recover an area-weighted heat flux. The area-weighted data were utilized in this work. The reader is referred to [3,48] for more detailed information about data processing, *i.e.* outlier elimination, filtering, and area-averaging.

The heat flux data were measured on a standard, uncoated metal piston. Global heat transfer measurements with coated and uncoated pistons [3] did not indicate a significant change to heat transfer for any of the coated pistons. Therefore, utilizing the metal piston heat flux data as an estimate for the heat flux to a coated piston was considered reasonable for the purpose of developing the fracture mechanics model.

Appendix B. Outline of the stress analysis and energy release rate calculations

The proposed mechanics technique assumes that the time is takes a stress wave (traveling with the speed of sound) to propagate through the wall is considerably faster than for the temperature to change; *i.e.* dynamic stresses are neglected. As such, the conduction heat transfer problem is unsteady while the mechanical problem is quasi-steady.

The state of deformation is different prior to and during the delamination process. Equi-biaxial deformation is taken for the pre-delamination process, while plane strain is assumed for the delamination process. The corresponding controlling moduli and effective thermal strain coefficients of each stress/deformation state are given in Table B.4.

By solving the constitutive law for two-dimensions, $\epsilon_x = \frac{1}{E}\left[\sigma_x - \nu\left(\sigma_y + \sigma_z\right)\right] + \vartheta$ and $\epsilon_z = \frac{1}{E}\left[\sigma_z - \nu\left(\sigma_x + \sigma_y\right)\right] + \vartheta$, the state of stress at any instant in an engine cycle, depth, and direction is given by

$$\sigma_x(y) = \frac{E}{1-\nu^2}\left[\epsilon_x + \nu\epsilon_z - (1-\nu)\vartheta\right] \tag{B.1}$$

$$\sigma_z(y) = \frac{E}{1-\nu^2}\left[\epsilon_z + \nu\epsilon_x - (1-\nu)\vartheta\right] \tag{B.2}$$

with total strains varying through the multilayer according to

$$\epsilon_x = \epsilon_{o,x} - \kappa_x y \tag{B.3}$$

and

$$\epsilon_z = \epsilon_{o,z} - \kappa_z\left(y + H_b\right) \tag{B.4}$$

where $\epsilon_{o,x}$, $\epsilon_{o,z}$ and κ_x, κ_z are the elongation and curvature of the x- and z-direction, respectively. The bottom sub-multilayer height is denoted as H_b. The thermal strain distribution ϑ is defined as

$$\vartheta(y) = \alpha\left(t(y) - t^{\mathrm{ref}}(y)\right) \tag{B.5}$$

where α is the thermal expansion coefficient, $t\,(y)$ is the current temperature distribution, and $t^{\text{ref}}\,(y)$ is the reference temperature distribution.

The reference or stress-free temperature defines the state at which the multilayer is at a relaxed, stress-free condition. In practice, this is defined by the temperature at which the substrate is pre-heated prior to coating deposition. The effect of the residual stresses may be an important control parameter for combustion engine coating design.

The mechanical system response initially estimates the elongation and curvature of the system using the steps illustrated below. Let ϑ_t^i and ϑ_b^i be the thermal strain at the top and bottom node of element i, respectively. Assuming a piece-wise linear distribution through each element i, one gets

$$\vartheta^i\,(y) = \vartheta_b^i + \frac{y - y_b^i}{y_t^i - y_b^i}\left(\vartheta_t^i - \vartheta_b^i\right) \tag{B.6}$$

where y_t^i and y_b^i is the position of the top and bottom of element i, respectively.

Force and moment equilibria in the absence of external loads, for a N number of nodes system, require that

$$\sum_{i=1}^{N}\int_{y_b^i}^{y_t^i}\sigma_x\left(y,\vartheta_b^i,\vartheta_t^i\right)dy = 0 \tag{B.7}$$

and

$$\sum_{i=1}^{N}\int_{y_b^i}^{y_t^i} y\cdot\sigma_x\left(y,\vartheta_b^i,\vartheta_t^i\right)dy = 0 \tag{B.8}$$

which results in a set of two linear equations governing $\epsilon_{o,x}$ and κ_x

$$\begin{bmatrix} a_{11} & a_{12}\\ a_{21} & a_{22}\end{bmatrix}\begin{bmatrix}\epsilon_{o,x}\\ \kappa_x\end{bmatrix} = \begin{bmatrix} b_1\\ b_2\end{bmatrix} \tag{B.9}$$

where the a and b coefficients for solving (B.9) are given below

$$a_{11} = \sum_{i=1}^{N}\bar{E}_i\ell_i \tag{B.10}$$

$$a_{12} = a_{21} = -\sum_{i=1}^{N}\frac{\bar{E}_i\ell_i}{2}\left(y_t^i + y_b^i\right) \tag{B.11}$$

$$a_{22} = \sum_{i=1}^{N}\frac{\bar{E}_i\ell_i}{3}\left[\left(y_t^i\right)^2 + y_t^i y_b^i + \left(y_b^i\right)^2\right] \tag{B.12}$$

$$\begin{aligned} b_1 = \sum_{i=1}^{N}\Bigg[&\frac{\bar{c}_i\bar{E}_i\ell_i}{2}\left(\vartheta_t^i + \vartheta_b^i\right) - \bar{E}_i\ell_i\nu_i\epsilon_{o,z}\\ &+\frac{\bar{E}_i\ell_i}{2}\left(y_t^i + y_b^i + 2H_b\right)\nu_i\kappa_z\Bigg] \end{aligned} \tag{B.13}$$

$$\begin{aligned} b_2 = -\sum_{i=1}^{N}\Bigg\{&+\frac{\bar{c}_i\bar{E}_i\ell_i}{6}\left[y_b^i\left(2\vartheta_b^i + \vartheta_t^i\right) + y_t^i\left(\vartheta_b^i + 2\vartheta_t^i\right)\right]\\ &+\frac{\nu_i\bar{E}_i\ell_i}{2}\left(y_t^i + y_b^i\right)\left(\epsilon_{o,z} - \kappa_z H_b\right)\\ &+\frac{\nu_i\bar{E}_i\ell_i}{3}\left[\left(y_t^i\right)^2 + y_t^i y_b^i + \left(y_b^i\right)^2\right]\Bigg\} \end{aligned} \tag{B.14}$$

where

$$\ell_i = y_t^i - y_b^i \tag{B.15}$$

such that

$$y_t^i = \sum_{p=1}^{i}\ell_p \qquad y_b^i = \sum_{p=1}^{i-1}\ell_p \qquad y_b^1 = 0 \tag{B.16}$$

Although similar a coefficients can be found in [9,44], the b coefficients are unique to the problem of equi-biaxial stress prior to delamination followed by plane strain after delamination. The a coefficients depend on the element effective moduli $\bar{E}_i$ and position $y_{t/b}^i$, and the b coefficients additionally are functions of the thermal strain ϑ^i, its coefficient $\bar{c}_i$ and the z-direction elongation and curvature and the bottom sub-multilayer height H_b. The elongation $\epsilon_{o,x}$ and curvature κ_x are determined by solving the linear system in Eq. (B.9) together with Eqs. (B.6) and (B.10)–(B.16).

Crack growth is initiated when the energy release rate overcomes fracture toughness.

$$G \geq G_c \tag{B.17}$$

The change in strain energy is directly related to the energy release rate. The strain energy, U_i, contained in element i is found from

$$U_i = \int_{y_b^i}^{y_t^i} \left[\frac{1+\nu}{2E} \left(\sigma_x^2 + \sigma_z^2 \right) - \frac{\nu}{2E} \left(\sigma_x + \sigma_z \right)^2 \right] dy \tag{B.18}$$

Combining the thermal strain distribution $\vartheta(y)$ from Eq. (B.6) and both stress components $\sigma_x(y)$ and $\sigma_z(y)$ as a function of position from Eq. (B.1) and (B.2) one gets

$$\begin{aligned}
U_i = {} & \frac{E_i \ell_i}{2\left(1-\nu^2\right)} \left[\epsilon_{o,x}^2 + \epsilon_{o,z}^2 + 2\nu \epsilon_{o,x} \epsilon_{o,z} \right. \\
& \left. - \left(2\nu \epsilon_{o,x} + 2\epsilon_{o,z} - \kappa_z H_b \right) \kappa_z H_b \right] \\
& - \frac{E_i \ell_i}{2\left(1-\nu^2\right)} \left(y_t^i + y_b^i \right) \left[\epsilon_{o,x} \left(\kappa_x + \nu \kappa_z \right) \right. \\
& \left. + \left(\epsilon_{o,z} - \kappa_z H_b \right) \left(\kappa_z + \nu \kappa_x \right) \right] \\
& + \frac{E_i \ell_i}{6\left(1-\nu^2\right)} \left[\left(y_t^i \right)^2 + y_t^i y_b^i + \left(y_b^i \right)^2 \right] \left(\kappa_x^2 + \kappa_z^2 + 2\nu \kappa_x \kappa_z \right) \\
& - \frac{E_i \ell_i}{2(1-\nu)} \left[\left(\vartheta_t^i + \vartheta_b^i \right) \left(\epsilon_{o,x} + \epsilon_{o,z} \right) - 2\vartheta_b \kappa_z H_b \right] \\
& + \frac{E_i \ell_i}{6(1-\nu)} \left\{ \left[y_b^i \left(2\vartheta_b^i + \vartheta_t^i \right) + y_t^i \left(\vartheta_b^i + 2\vartheta_t^i \right) \right] \left(\kappa_x + \kappa_z \right) \right. \\
& \left. + 3 \left(\vartheta_t^i - \vartheta_b^i \right) \kappa_z H_b \right\} \\
& + \frac{E_i \ell_i}{3(1-\nu)} \left[\left(\vartheta_b^i \right)^2 + \vartheta_b^i \vartheta_t^i + \left(\vartheta_t^i \right)^2 \right]
\end{aligned} \tag{B.19}$$

The energy release rate G at any interior location is determined by the difference between the strain energy of the intact (whole) multilayer ahead of the crack and the total strain energy contained in the two (top and bottom) layers formed by the crack interface, such as

$$G = U^{\text{whole}} - \left(U^{\text{top}} + U^{\text{bottom}} \right) \tag{B.20}$$

where U^{whole} and $\left(U^{\text{bottom}} + U^{\text{top}} \right)$ is the strain energy of the intact multilayer and the strain energy sum of the piston substrate, U^{bottom}, and coating, U^{top} (top), respectively.

References

[1] Myers PS. Ceramics for transportation engines—siren or solution. Appl Mech Rev 1989. http://dx.doi.org/10.1115/1.3152421.

[2] Hendricks TL. Instantaneous heat flux measurements in internal combustion engines (Ph.D. thesis), University of Wisconsin-Madison; 2011, 2011, URL http://digital.library.wisc.edu/1793/79399.

[3] Gingrich E. High-output diesel engine heat transfer (Ph.D. thesis), University of Wisconsin-Madison; 2020, URL https://apps.dtic.mil/sti/citations/AD1109699.

[4] Sundaram S, Lipkin D, Johnson C, Hutchinson JW. The influence of transient thermal gradients and substrate constraint on delamination of thermal barrier coatings. J Appl Mech 2013;80(1). http://dx.doi.org/10.1115/1.4007727.

[5] Evans A, Hutchinson J. The mechanics of coating delamination in thermal gradients. Surf Coat Technol 2007;201(18):7905–16. http://dx.doi.org/10.1016/j.surfcoat.2007.03.029.

[6] Krämer S, Faulhaber S, Chambers M, Clarke DR, Levi CG, Hutchinson JW, et al. Mechanisms of cracking and delamination within thick thermal barrier systems in aero-engines subject to calcium-magnesium-alumino-silicate (CMAS) penetration. Mater Sci Eng A 2008;490(1–2):26–35. http://dx.doi.org/10.1016/j.msea.2008.01.006.

[7] Xue Z, Evans A, Hutchinson J. Delamination susceptibility of coatings under high thermal flux. J Appl Mech 2009;76(4). http://dx.doi.org/10.1115/1.3086590.

[8] Levi CG, Hutchinson JW, Vidal-Sétif M, Johnson CA. Environmental degradation of thermal-barrier coatings by molten deposits. MRS Bull 2012;37(10):932–41. http://dx.doi.org/10.1557/mrs.2012.230.

[9] Jackson RW, Begley MR. Critical cooling rates to avoid transient-driven cracking in thermal barrier coating (TBC) systems. Int J Solids Struct 2014;51(6):1364–74. http://dx.doi.org/10.1016/j.ijsolstr.2013.12.029.

[10] Staroselsky A, Martin TJ, Borkowski L. The influence of thermal transient rates on coated turbine parts' life expectancy. J Eng Gas Turbines Power 2019;141(4). http://dx.doi.org/10.1115/1.4041110.

[11] Evans AG, Mumm D, Hutchinson J, Meier G, Pettit F. Mechanisms controlling the durability of thermal barrier coatings. Prog Mater Sci 2001;46(5):505–53. http://dx.doi.org/10.1016/S0079-6425(00)00020-7.

[12] Uchida N. A review of thermal barrier coatings for improvement in thermal efficiency of both gasoline and diesel reciprocating engines. Int J Engine Res 2020. http://dx.doi.org/10.1177/1468087420978016.

[13] Kamo R. Adiabatic turbocompound engine performance prediction. SAE technical papers, 1978, http://dx.doi.org/10.4271/780068.

[14] Bryzik W, Kamo R. TACOM/Cummins Adiabatic engine program. SAE Trans 1983;1063–87, URL https://www.jstor.org/stable/44644435.

[15] Kamo R, Bryzik W. Cummins/TACOM advanced adiabatic engine. In: Ceram. eng. sci. proc. Vol. 5. Wiley Online Library; 1984, p. 312–38, URL https://www.jstor.org/stable/44467034.

[16] Woschni G, Spindler W, Kolesa K. Heat insulation of combustion chamber walls—a measure to decrease the fuel consumption of IC engines? SAE Trans 1987;269–79, URL https://www.jstor.org/stable/44470841.
[17] Cheng WK, Wong VW, Gao F. Heat transfer measurement comparisons in insulated and non-insulated diesel engines. SAE technical paper, SAE Technical Paper; 1989, http://dx.doi.org/10.4271/890570.
[18] Morel T, Keribar R, Blumberg PN. Cyclical thermal phenomena in engine combustion chamber surfaces. SAE technical paper series, 1985, http://dx.doi.org/10.4271/850360.
[19] Assanis DN, Heywood JB. Development and use of a computer simulation of the turbocompounded diesel system for engine performance and component heat transfer studies. SAE International; 1986, http://dx.doi.org/10.4271/860329.
[20] Kamo R, Assanis DN, Bryzik W. Thin thermal barrier coatings for engines. SAE Trans 1989;131–6.
[21] Kosaka H, Wakisaka Y, Nomura Y, Hotta Y, Koike M, Nakakita K, et al. Concept of temperature swing heat insulation in combustion chamber walls, and appropriate thermo-physical properties for heat insulation coat. SAE Int J Engines 2013;6(1):142–9. http://dx.doi.org/10.4271/2013-01-0274.
[22] Wakisaka Y, Inayoshi M, Fukui K, Kosaka H, Hotta Y, Kawaguchi A, et al. Reduction of heat loss and improvement of thermal efficiency by application of temperature swing insulation to direct-injection diesel engines. SAE Int J Engines 2016;9(3):1449–59. http://dx.doi.org/10.4271/2016-01-0661.
[23] Kawaguchi A, Iguma H, Yamashita H, Takada N, Nishikawa N, Yamashita C, et al. Thermo-swing wall insulation technology; - a novel heat loss reduction approach on engine combustion chamber. SAE technical paper series, 2016, http://dx.doi.org/10.4271/2016-01-2333.
[24] Kawaguchi A, Wakisaka Y, Nishikawa N, Kosaka H, Yamashita H, Yamashita C, et al. Thermo-swing insulation to reduce heat loss from the combustion chamber wall of a diesel engine. Int J Engine Res 2019. http://dx.doi.org/10.1177/1468087419852013.
[25] Koutsakis G, Miles S, Ghandhi J. Assessment of in-cylinder thermal barrier coatings over a full vehicle drive cycle. SAE Int 2021. http://dx.doi.org/10.4271/2021-01-0456.
[26] Yonushonis TM. Thick thermal barrier coatings for diesel components. NASA Lewis Research Center; 1991.
[27] Saad D, Saad P, Kamo L, Mekari M, Bryzik W, Schwarz E, et al. Thermal barrier coatings for high output turbocharged diesel engine. SAE technical paper, 2007, http://dx.doi.org/10.4271/2007-01-1442.
[28] Tricoire A, Kjellman B, Wigren J, Vanvolsem M, Aixala L. Insulated piston heads for diesel engines. J Therm Spray Technol 2009;18(2):217–22. http://dx.doi.org/10.1007/s11666-009-9301-x.
[29] Uchida N, Osada H. A new piston insulation concept for heavy-duty diesel engines to reduce heat loss from the wall. SAE Int J Engines 2017;10(5):2565–74. http://dx.doi.org/10.4271/2017-24-0161.
[30] de Goes WU, Somhorst J, Markocsan N, Gupta M, Illkova K. Suspension plasma-sprayed thermal barrier coatings for light-duty diesel engines. J Therm Spray Technol 2019;28(7):1674–87. http://dx.doi.org/10.1007/s11666-019-00923-8.
[31] Thibblin A, Kianzad S, Jonsson S, Olofsson U. Running-in behaviour of thermal barrier coatings in the combustion chamber of a diesel engine. Proc Inst Mech Eng D 2019. http://dx.doi.org/10.1177/0954407019841173.
[32] Thibblin A, Olofsson U. A study of suspension plasma-sprayed insulated pistons evaluated in a heavy-duty diesel engine. Int J Engine Res 2020;21(6):987–97. http://dx.doi.org/10.1177/1468087419879530.
[33] Powell T, O'Donnell R, Hoffman M, Filipi Z, Jordan EH, Kumar R, et al. Experimental investigation of the relationship between thermal barrier coating structured porosity and homogeneous charge compression ignition engine combustion. Int J Engine Res 2019. http://dx.doi.org/10.1177/1468087419843752.
[34] Buyukkaya E, Cerit M. Thermal analysis of a ceramic coating diesel engine piston using 3-D finite element method. Surf Coat Technol 2007;202(2):398–402. http://dx.doi.org/10.1016/j.surfcoat.2007.06.006.
[35] Cerit M. Thermo mechanical analysis of a partially ceramic coated piston used in an SI engine. Surf Coat Technol 2011;205(11):3499–505. http://dx.doi.org/10.1016/j.surfcoat.2010.12.019.
[36] Moridi A, Azadi M, Farrahi G. Thermo-mechanical stress analysis of thermal barrier coating system considering thickness and roughness effects. Surf Coat Technol 2014;243:91–9. http://dx.doi.org/10.1016/j.surfcoat.2012.02.019.
[37] Bayata F, Yildiz C. The analyses of frictional losses and thermal stresses in a diesel engine piston coated with different thicknesses of thermal barrier films using co-simulation method. Int J Engine Res 2021. http://dx.doi.org/10.1177/14680874211065637.
[38] Zhu D, Miller RA. Investigation of thermal high cycle and low cycle fatigue mechanisms of thick thermal barrier coatings. Mater Sci Eng A 1998;245(2):212–23. http://dx.doi.org/10.1016/S0921-5093(97)00852-6.
[39] Baldissera P, Delprete C. Finite element thermo-structural methodology for investigating diesel engine pistons with thermal barrier coating. SAE Int J Engines 2019;12(1):69–78. http://dx.doi.org/10.4271/03-12-01-0006.
[40] Pierz P. Thermal barrier coating development for diesel engine aluminum pistons. Surf Coat Technol 1993;61(1–3):60–6. http://dx.doi.org/10.1016/0257-8972(93)90203-Z.
[41] Zhu D, Miller RA. Influence of high cycle thermal loads on thermal fatigue behavior of thick thermal barrier coatings. Tech. rep., Cleveland, Ohio: NASA; 1997.
[42] Beardsley MB. Potential use of quasicrystalline materials as thermal barrier coatings for diesel engine components. Iowa State University; 2008.
[43] Moser S. Coupled thermal mechanical analysis methodology for thermal performance evaluation and failure mode identification of thermal barrier coatings for heavy duty diesel engines (Ph.D. thesis), Clemson University; 2021.
[44] Begley MR, Hutchinson JW. The mechanics and reliability of films, multilayers and coatings. Cambridge University Press; 2017.
[45] Hendricks TL, Splitter DA, Ghandhi JB. Experimental investigation of piston heat transfer under conventional diesel and reactivity-controlled compression ignition combustion regimes. Int J Engine Res 2014;15(6):684–705.
[46] Nellis G, Klein S. Heat transfer. Cambridge University Press; 2009.
[47] Koutsakis G, Nellis GF, Ghandhi JB. Surface temperature of a multi-layer thermal barrier coated wall subject to an unsteady heat flux. Int J Heat Mass Transfer 2020;155. http://dx.doi.org/10.1016/j.ijheatmasstransfer.2020.119645.
[48] Gingrich E, Tess M, Korivi V, Ghandhi J. High-output diesel engine heat transfer: Part 1 - comparison between piston heat flux and global energy balance. Int J Engine Res 2021. http://dx.doi.org/10.1177/14680874211017032.
[49] Saputo J. Personal communication with Stony Brook University. 2021.
[50] Gingrich E, Tess M, Korivi V, Schihl P, Saputo J, Smith GM, et al. The impact of piston thermal barrier coating roughness on high-load diesel operation. Int J Engine Res 2019. http://dx.doi.org/10.1177/1468087419893487.
[51] Saputo JC, Smith GM, Lee H, Sampath S, Gingrich E, Tess M. Thermal swing evaluation of thermal barrier coatings for diesel engines. J Therm Spray Technol 2021;1–15. http://dx.doi.org/10.1007/s11666-020-01117-3.
[52] Chen Y-C, Worden JA. Evaluation of microalloyed steel for articulated piston applications in heavy duty diesel engines. Tech. rep., SAE Technical Paper; 2000, http://dx.doi.org/10.4271/2000-01-1232.
[53] Granta Selector. ANSYS, INc. 2020.